

# Wildfire Risk Metric Impact on Public Safety Power Shut-off Cost Savings

Ryan Greenough, Kohei Murakami, Jan Kleissl, and Adil Khurram

**Abstract**—Public Safety Power Shutoffs (PSPS) are a proactive strategy to mitigate fire hazards from power system infrastructure failures. System operators employ PSPS to deactivate portions of the electric grid with heightened wildfire risks to prevent wildfire ignition and redispatch generators to minimize load shedding. A measure of vegetation flammability, called the Wildland Fire Potential Index (WFPI), has been widely used to evaluate the risk of nearby wildfires to power system operation. However, the WFPI does not correlate as strongly to historically observed wildfire ignition probabilities (OWIP) as WFPI-based the Large Fire Probability (WLFP). Prior work chose not to incorporate wildfire-driven failure probabilities, such as the WLFP, because constraints with Bernoulli random variables to represent wildfire ignitions could require non-linear or non-convex constraints. This paper uses a deterministic equivalent of an otherwise complicating line de-energization constraint by quantifying the wildfire risk of operating transmission line as a sum of each energized line’s wildfire ignition log probability ( $\log(\text{WIP})$ ) rather than as a sum of each energized line’s WFPI. A day-ahead unit commitment and line de-energization PSPS framework is used to assess the cost differences driven by the choice between the WFPI and WLFP risk metrics. Training the optimization on scenarios developed by mapping WLFP to  $\log(\text{WIP})$  rather than mapping the WFPI to  $\log(\text{WIP})$  leads to reductions in the total real-time costs. For the IEEE RTS 24-bus test system, mapping transmission line WLFP values to  $\log(\text{WIP})$  resulted in a 14.8% (on average) decrease in expected real-time costs.

**Index Terms**—Day-ahead unit commitment, extreme weather events, optimal power flow, Public Safety Power Shut-offs & wildfire risk mitigation

## I. INTRODUCTION

The California Department of Forestry and Fire Protection (CalFire) reports that 95% of wildfires in California are caused by human activity including electrical failures, campfires, debris burning, smoking, and arson [1]. Transmission line failures account for less than 10% of reported wildfire ignitions in California [2]. Yet, seven of California’s most destructive wildfires were caused by power lines [1]. To prevent energized electrical equipment from igniting new wildfires while also ensuring reliable electrical grid operation during ongoing or potential wildfires without putting the public at risk, electric utilities execute Public Safety Power Shutoff (PSPS) [3]. The California Public Utilities Commission (CPUC) defines PSPS as the act of utilities temporarily turning off power to

specific areas to reduce the risk of fires caused by electric infrastructure [2].

A significant challenge to operators during PSPS is to coordinate equipment de-energizations to minimize load shed as well as wildfire ignition and spread. Common planning approaches, such as the N-1 security-constrained approach, may not be helpful in PSPS since several power lines may intersect the region near a large wildfire. Instead N-k contingencies based approach are more suitable but are computationally expensive because the feasibility set grows combinatorially with k, which is the number of de-energized components.

PSPS has been formulated as a deterministic problem [4]–[8], [11], [12] and as a stochastic problem [9], [10], [13]. And wildfire-related impacts to the grid are often included in the PSPS optimization problem as an exogenous input that can affect optimization parameters such as wildfire damage costs, transmission line outage probabilities, and thermal limits on transmission line power flow.

[11]–[13] create wildfire forecasting models to enhance the optimization of PSPS decisions. [11] trains a neural network model for forecasting spatio-temporal wildfire risk using features such as vegetation level, dry fuel, wind speed, and the type of geographical terrain. [12], [13] contribute a wildfire forecasting surrogate that approximates the non-linear PDEs describing the droop dynamics of transmission lines using the Runge-Kutta method which is then used to make a wildfire risk score prediction. [12], [13] then implement the wildfire risk score as an input to a deterministic PSPS model, called the wildfire risk-aware operation planning problem or WRAP, to determine operational decisions. [12] shows cost reductions from using the wildfire risk score surrogate in place of the assignment of NOAA’s Fire Weather Threat to power lines (e.g. wildfire risk values from 1-5) performed in [5]. [12], [13] do not compare the optimal costs resulting from using their wildfire risk score to the optimal costs from more accepted wildfire risk metrics, such as WFPI forecasts.

[6]–[10] simplified the prediction of wildfire risk by defining wildfire risk as a deterministic exogenous input to the optimization model and assigning a wildfire risk directly to each active power system component. And similar to what is done in [4], [6]–[13], we are only accounting for the wildfire risk of operating transmission lines.

Extensions of the OPS model shifted the characterization of line wildfire risk to represent a US Geological Survey’s (USGS) normalized vegetation flammability index, called the Wildland Fire Potential Index (WFPI) [6]–[10]. WFPI describes the ratio of live to dead fuel to quantify wildfire risk and can be linked to historically observed wildfire ignition.

Ryan Greenough, Kohei Murakami, and Adil Khurram are with the Department of Mechanical and Aerospace Engineering, University of California at San Diego, La Jolla, CA 92093 USA (e-mail: rgreenou@ucsd.edu; k1murakami@ucsd.edu; akhurram@ucsd.edu)

Jan Kleissl is with the Center for Energy Research, Department of Mechanical and Aerospace Engineering, University of California at San Diego, La Jolla, CA 92093 USA (e-mail: jkleissl@ucsd.edu).

[6]–[10] determine that it is more practical to use WFPI forecasts than NOAA fire warnings to operationally model a wildfire’s impact as NOAA fire warnings are not granular enough. Historical WFPI observations are advantageous by offering a finer resolution of historically observed wildfire ignition probabilities among large wildfires. WFPI integer values range from 0 to 150 and can be mapped to a continuous range of wildfire ignition probability (WIP). [6]–[10] pull input WFPI forecasts directly into the PSPS optimization. However, [6]–[8] average the top 10% of all WFPI values experienced by the transmission lines over the 2019 and 2020 wildfire seasons. This approach overestimates the wildfire risk in the network compared to using the real-time WFPI values, as done in [10], and may lead to higher costs due to over-committing generating resources in anticipation of more line de-energizations.

OPS as defined in [5]–[9] assumes an operator optimally serves demand and de-energizes transmission lines through a bi-objective function that balances maximizing the total demand served with minimizing total system wildfire risk. This differs philosophically from [11] who minimizes load shed and assumes a system operator’s energization decisions do not contribute to wildfire spread. [11] also does not consider uncertainty in nodal energy demands. In [5]–[8], [10], the total system wildfire risk is the sum of wildfire risks assigned to each energized line. The OPS model in [5]–[8] is deterministic, does not consider commitment and operational costs, and does not develop a methodology for selecting appropriate weights for trading off max-normalized load shed versus max-normalized WFPI wildfire risk. In practice, there is uncertainty in wildfire ignition and its subsequent spread which motivates probabilistic wildfire models. [9] extends OPS to a two-stage stochastic mixed integer program (SMIP) to model the operational PSPS decisions over the evolution of simulated wildfire events. However, there is no consideration of unit commitment strategies for the generators.

In the authors’ previous work [10], a mean-Conditional Value at Risk (mean-CVaR) two-stage stochastic unit commitment problem was developed to study the impact of uncertain demand on unit commitment and line de-energization decisions. Unlike [5]–[9], [10] frames the optimization purely in terms of economic costs as the sum of unit commitment and operational costs instead of only the Value of Lost Load (VoLL) costs [5]–[8] and wildfire damage costs [9]. Furthermore, [6]–[10] do not investigate different wildfire risk metrics.

The USGS website provides a depiction of how well WFPI and WLFP forecasts are related to the historically observed fraction of ignited voxels by large wildfires expressed as historically observed large wildfire ignition probabilities (OWIP) [15]). More large fires occurred at the highest levels of WFPI; however, there is a large scatter in the distribution that maps large WFPI to OWIP. This large scatter in the relationship between large WFPI values and observed ignition probabilities can affect the OPS decision-making. For instance, a significant underestimation of the real-time wildfire risk could lead to day-ahead generation commitment that results in higher real-time generation costs. [6]–[10] do not incorpo-

rate any uncertainty in WFPI forecasts. To account for the uncertainty in the prediction of large wildfires, we suggest a probabilistic approach to PSPS optimization with wildfire-related parameters. In this work, we use the USGS WLFP to estimate transmission line wildfire risk because WLFP is more correlated to OWIP than WFPI. We assume operators make decisions based on economic costs, and operators use a tolerance level,  $\pi_{\text{tol}}$ , for an allowable probability of damage to transmission lines.

In this work, we modify the deterministic version of the Stochastic PSPS (SPSPS) proposed in [10]. In contrast to the author’s earlier work, we model wildfire ignitions as Bernoulli random events and compare PSPS costs resulting from mapping WFPI and WLFP forecasts to WIP respectively.

The optimization is solved in two stages. In the day ahead, unit commitment decisions are optimized based on the inputs of expected total demand at each bus and the expected observed wildfire ignition probability for each line with respect to the probability of the five representative daylong scenarios. Then optimized expected power flow and power injections are determined in real-time for the IEEE RTS 24-bus transmission grid and the day-ahead unit commitment decisions are tested on multiple line damage scenarios via a Monte Carlo simulation. Within the Monte Carlo simulation, we use real-time demand and a collection of transmission line outage scenarios based on the real-time WIP forecast near transmission lines. Then we discuss the trend in increased optimized commitment and operational costs resulting from WFPI-based forecasts as opposed to WLFP-based forecasts.

The main contributions of this paper are the following:

- 1) To the best of our knowledge, this is the first paper to illustrate and quantify potential drawbacks of using the WFPI instead of WLFP to quantify the power systems operating risks related to nearby wildfires. We illustrate that not only does WLFP map more accurately to OWIP than WFPI during peak wildfire season, but also demonstrate the cost savings for the PSPS model by incorporating wildfire ignition probabilities (WIP) mapped from WLFP forecasts instead of from WFPI forecasts.
- 2) We use real-time transmission line WIP to directly simulate transmission line failure scenarios during PSPS events without relying on the association between WFPI and potential real-time damages to transmission lines (as needed in the OPS model in [6]–[9]).
- 3) We extend the day-ahead unit commitment model proposed in [10] by modifying the constraint on allowable wildfire risk to be robust to a wildfire ignition’s Bernoulli uncertainty rather than directly inputting deterministic wildfire forecasts.

The paper is organized as follows. We reiterate that we use a special case of SPSPS that is deterministic. Section II explains the methodology behind using WLFP to forecast WIP rather than WFPI. Section III introduces all elements of the Public Safety Power Shut-off (PSPS) strategy including the day-ahead and real-time formulations. Section IV explains the results of the unit commitment for WFPI and WLFP on an IEEE RTS 24-bus system. Section V concludes the paper.

## II. SELECTION OF WILDFIRE RISK METRIC

### A. Example comparison

The Wildland fire potential index (WFPI) has been used extensively in recent research works, e.g. [5]–[10], to assess the risk of damage to power system components from nearby wildfires. This metric describes the ratio of live to dead fuel and includes variables for wind speed, dry bulb temperature, and rainfall [16]. WFPI values range from 0 to 150. Values of 249–254 mark land outside the United States, ice, agricultural land, barren land, marshland, and bodies of water; all terrain conditions with WFPI values from 249 – 254 are considered to have zero WFPI. In [6]–[10], day-ahead forecasts of WFPI are taken directly from the USGS database.

The USGS has also developed the WLFP to estimate the risk that a new fire will burn more than 500 acres [17]. Probabilities in WLFP are assigned per million voxels where 1 voxel is equal to an area of 1 km<sup>2</sup>. The WLFP forecasts are derived from historical average probabilities of large fires and are adjusted based on the WFPI of that day [17]. The USGS generates WFPI and WLFP forecasts for the continental US up to seven days in the future. Both of the USGS’s WFPI and WLFP forecasting models are validated through tests using historical fire incidence data from [18].

From the USGS fire data products page, a collection of one-day-ahead forecasts (saved in .tiff format) is downloaded and combined to form timeseries of WLFP and WFPI predictions for each of the 24 locations of the IEEE RTS 24-bus. Each .tiff file contains a grid mesh in which each grid point has a WLFP and WFPI value and a pixel  $x$ - $y$  coordinate. Each pixel coordinate is translated into a coordinate with a longitude and latitude. Since the precision of the bus longitude/latitude is finer than the resolution of the .tiff file, the four nearest neighbors from the .tiff grid mesh are averaged to form the forecast of the bus location. The Bresenham’s line algorithm is used to collect grid points near the transmission lines. A collection of WFPI/WLFP values is assigned to each transmission line,  $(i, j)$ , via the Bresenham algorithm [20] and the buses at the ends of the lines. A depiction of average WLFP bus and line values, recorded on July 31st, 2020, on the IEEE 24-bus RTS system in Southern California, is depicted in Figure 1.

However, we show that periods of elevated WFPI do not align as well with periods of elevated observed wildfire ignitions as do periods of elevated WLFP. Figure 2 shows the seven-day moving averages (MA) of time series for the WFPI (top) and WLFP (bottom) near bus 23 in the IEEE RTS 24-bus system sampled daily in 2015. The Lake Fire was the largest wildfire in Southern California in 2015 (31,359 acres burned); it started near San Bernardino on June 17 and lasted until August 1. Bus 23 is the closest bus in the IEEE RTS 24-bus to the fire’s spread. In figure 2, the 7-day moving average of both WFPI and WLFP increases sharply from around June 11th to June 22nd (6 six days before to 5 days after the start of the Lake Fire). There is a 307% in WLFP and a 36% increase in WFPI. The three peaks in WLFP during the Lake Fire are the 1st, 2nd, and 22nd highest MA WLFP values of the year. All values during the Lake Fire are within the 64th percentile of WLFP values experienced that year. The three peaks in WFPI

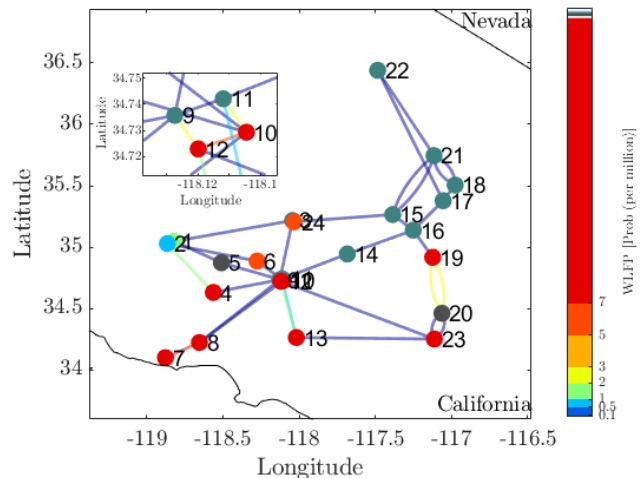


Fig. 1: Schematic of the IEEE RTS 24-bus system with each transmission line and bus highlighted to depict its WLFP for July 31st, 2020. The geographic layout comes from [21]. Zero-risk buses are 3, 5, 9, 11, 14-18, 20-22 and zero-risk lines are 14, 23-26, 28, 30-33, 38. There are four line pairs: 25/26, 32/33, 33/34, and 36/37 in which each line in a pairing is assumed to have the same risk.

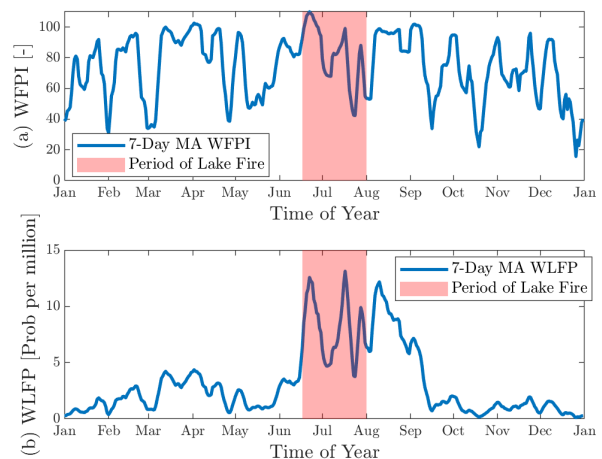


Fig. 2: A comparison of time series of the 7-day moving average of WFPI (a) and WLFP (b) for node 23 on the IEEE RTS 24-bus system near San Bernardino [16] in 2015. The transparent red region indicates the time-span of the largest fire in San Bernardino in 2015, the Lake Fire.

during the Lake Fire are the 1st, 26th, and 105th highest MA WFPI values of the year. There are values of WFPI during the Lake Fire as low as the 8th percentile of WFPI values experienced during 2015. There are reported WFPI values in the 80th and 90th percentile of 2015 during March, April, and May. In 2015, no wildfires occurred in that region of Southern California in March and May. Only one wildfire exceeding 1,000 acres (1,049 acres burned) occurred in Riverside from the 18th to the 24th of April [19]. We conclude anecdotally that WLFP values are more correlated to observed large wildfires than WFPI values.

The USGS provides reliability diagrams for both WFPI

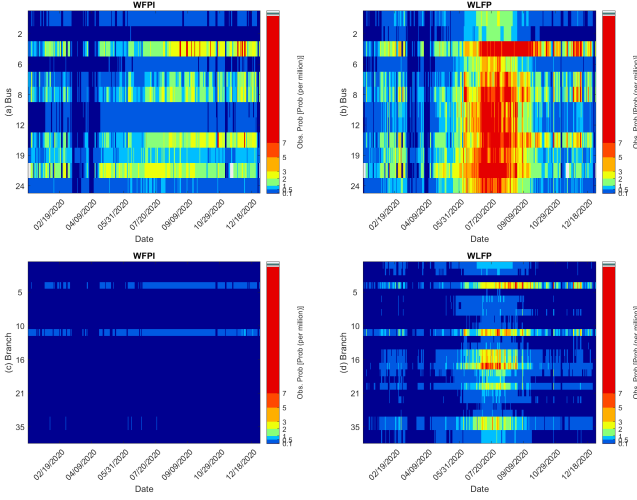


Fig. 3: Comparison of time series of the WIP predicted from WFPI (a) & (c) and WLFP (b) & (d) near each bus (a) & (b) and along each of the transmission lines (c) & (d) for the 24-bus Reliability Test System in 2020. Dates of elevated levels of WIP predicted from WLFP correspond more closely to increases in the historically observed large wildfire ignitions in Southern California than from WIP predicted from WFPI. Missing days of data in 2020 include April 14th, April 24th, and July 30th. Zero risk buses and lines are removed (Buses 3, 5, 9, 11, 14-18, 20-22 and lines 14, 23-26, 28, 30-33, 38).

(Table 1 and Figure 3 in [16]) and WLFP (Table 1 and Figure 2 in [17]). These reliability diagrams give distributions of yearly historically observed wildfire ignition probabilities for different ranges of WFPI or WLFP values. These observed wildfire ignition probabilities (OWIP) capture trends in historical wildfire occurrences from 1992 to 2020 [18]. For each WFPI/WLFP bus or line value, we project that value to an OWIP distribution based on the bins provided by the reliability diagrams. The mean of that conditional OWIP (i.e. OWIP given a WFPI or WLFP range) is used to represent the wildfire ignition probability (WIP) for that respective bus or line. Mean values for each conditional distribution are given in Table 1 in both [16] and [17]. These WIP values represent the bus or line wildfire risk and are inputted into the SPSPS problem as an exogenous input.

Figure 3 depict the mapping of all daily average bus and line WFPI and WLFP values observed in the year 2020 for the IEEE RTS 24-bus system [21] respectively to WIP values. Similar to what is seen for the WFPI forecast at Bus 23, yearly WIP forecasts predicted from WFPI do not qualitatively map to periods of elevated wildfire incidences during the main Summer wildfire season as consistently as WIP forecasts predicted from WLFP. The Southern California wildfire season is from late May to late September [14].

This qualitative analysis is strengthened by a comparison of similarity in the normalized distributions of the OWIP, WIP from WFPI, and WIP from WLFP.

## B. Comparison of WIP Distributions Generated from WFPI and WLFP Forecasts to Observed WIP Distributions

A bounding box (in Figure 4) is constructed to encompass all RTS IEEE 24-Bus System buses with at least a 0.2-degree longitude/latitude buffer. A K-means clustering is performed on the longitude and latitude of all fires from [18], inside the bounding box, and having burned more than 500 acres.

In Figure 4, a K-means clustering partitions the large wildfire data into 6 clusters. We exclude Cluster 2 and Cluster 4 from subsequent analysis. All buses in Cluster 2 (15-18 and 21-22) contain zero risk because they are located in either barren land or marshland [16]. Cluster 4 does not contain any buses from the IEEE RTS 24-bus system. Buses 3, 5, 9, 11, 14-18, and 20-22 have zero risk and are excluded from the mean absolute error analysis.

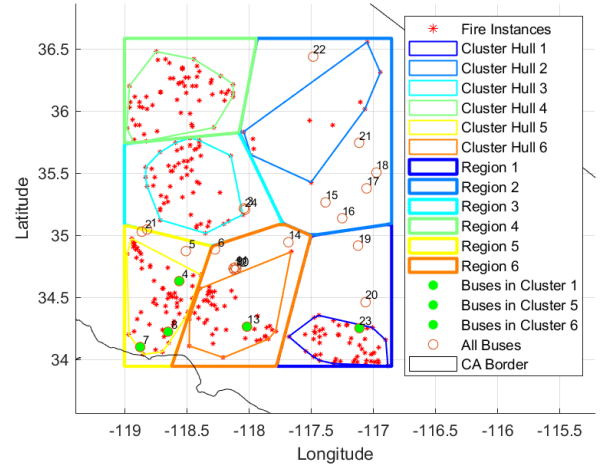


Fig. 4: K-Means clustering (K=6) of Wildfire Data from [18] needed to compute regional differences in wildfire spread nearby the IEEE 24-Bus System

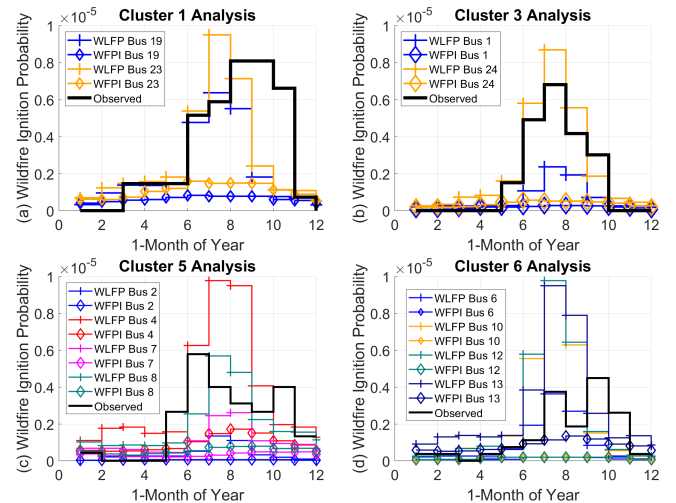


Fig. 5: Comparison of discrete distributions averaged from 2001 to 2020 and with a bin width of 1 month for WIP based on WFPI, WIP based on WLFP, and OWIP from [18]

We compute a sample averaged discrete distribution for each cluster to approximate each cluster's OWIP. We collect the start dates of all large wildfires within a cluster across the

20 years of the wildfire data (from 2001 to 2020). Then the probability of wildfire ignition in a given month is the number of counts normalized by the area of the convex hull of the cluster (in km<sup>2</sup>) times roughly 600 days (i.e. number of days in that month  $\times$  20 years). Each month block in the WIP timeseries data is averaged across 20 years. All bus WIPs within the  $i$ -th region are compared to the OWIP from the  $i$ -th cluster hull.

We compare the mean absolute error (MAE) between the yearly averaged WIP based on WFPI with the yearly averaged Observed WIP (OWIP) and MAE between yearly averaged WIP based on WLFP with yearly averaged OWIP. The MAE for each bus,  $b$ , or  $MAE_b$  is computed via Equation 1:

$$MAE_b = \frac{1}{12} \sum_{m=1}^{12} |WIP_{b,m} - OWIP_{k,m}| \quad \forall b \in \mathcal{B}_k \quad (1)$$

In (1), we determine the MAE for a given bus  $MAE_b$  by comparing its WIP to the OWIP of its corresponding cluster  $k$ . The absolute errors at each month are summed; the total absolute error is normalized by the number of months in a year. See Table I for the MAEs at every non-zero risk bus. For 8 out of the 12 buses (including all buses in Cluster 1 and Cluster 3), there is an improvement in MAE using WLFP to predict monthly WIP (on average 33.6%). At buses 4, 10, 12, and 13, the elevated levels of wildfire ignition probability in June, July, and August contributed to at least a 32% higher MAE from WIP based on WLFP than WFPI (65.5% on average higher MAE between those four cases). However, the MAE from WIP based on WLFP was less than the WFPI's WIP for more buses (8 buses had lower MAE w/ WLFP and 4 had lower MAE w/ WFPI), and the MAE w/ WLFP was less on all buses in Cluster 1 and 3. We observe that WLFP predicts OWIP more accurately than WFPI (12.2 % improvement in total MAE across all buses ).

Since WIP forecasts from WFPI did not capture the spatial and temporal trends in the observed wildfire ignition probabilities as well as WIP forecasts from WLFP from both a qualitative and MAE sense, we choose to determine de-energization decisions based on the WLFP rather than the WFPI. Moving forward, our analysis assumes that grid operators determine transmission line energizations by assessing the probability of large wildfire ignitions near transmission lines rather than the vegetation flammability indices near transmission lines.

### III. MODELING PSPS FOR WILDFIRE RISK MITIGATION

#### A. Preliminaries

Let  $\mathcal{P} = (\mathcal{B}, \mathcal{L})$  be the graph describing the power grid where  $\mathcal{B} = \{1, \dots, B\}$  is the set of  $B$  buses in the network, and  $\mathcal{L}$  is the set of edges such that two buses  $i, j \in \mathcal{B}$  are connected by a transmission line if  $(i, j) \in \mathcal{L}$ . The set of buses with generators and loads are collected in  $\mathcal{G}$  and  $\mathcal{D}$  respectively, and  $\mathcal{H} = \{1, \dots, H\}$  is the set of time indices over the horizon  $H$  of the optimization problem. A DC-OPF is used to approximate the line power flows and bus power injections; all references to power are to its active power. At any timestep  $t$ , the power injected by the generator at bus  $g \in \mathcal{G}$  in scenario  $\omega \in \Omega$  is denoted by  $p_{g,t,\omega}$ . Similarly,

TABLE I: Table of the Mean Absolute Errors between each bus's wildfire ignition probability (WIP) (derived from WFPI or WLFP) and the observed wildfire ignition probability (OWIP) and the percent improvement in MAE when using the WLFP versus WFPI. Distribution is averaged over 20 years and each bin width is one month.

Cluster 1	MAE WLFP	MAE WFPI	Improve %
Bus 19	$1.46 \times 10^{-6}$	$2.84 \times 10^{-6}$	48.7
Bus 23	$1.61 \times 10^{-6}$	$2.51 \times 10^{-6}$	35.9
Cluster 3	MAE WLFP	MAE WFPI	Improve %
Bus 1	$1.32 \times 10^{-6}$	$1.68 \times 10^{-6}$	21.6
Bus 24	$7.50 \times 10^{-7}$	$1.65 \times 10^{-6}$	54.4
Cluster 5	MAE WLFP	MAE WFPI	Improve %
Bus 2	$1.85 \times 10^{-6}$	$2.08 \times 10^{-6}$	11.2
Bus 4	$1.96 \times 10^{-6}$	$1.48 \times 10^{-6}$	-32.4
Bus 7	$1.39 \times 10^{-6}$	$1.89 \times 10^{-6}$	26.2
Bus 8	$1.22 \times 10^{-6}$	$1.74 \times 10^{-6}$	29.6
Cluster 6	MAE WLFP	MAE WFPI	Improve %
Bus 6	$7.31 \times 10^{-7}$	$1.27 \times 10^{-6}$	42.2
Bus 10	$1.84 \times 10^{-6}$	$1.24 \times 10^{-6}$	-48.2
Bus 12	$1.85 \times 10^{-6}$	$1.24 \times 10^{-6}$	-49.7
Bus 13	$1.98 \times 10^{-6}$	$8.51 \times 10^{-7}$	-132
All buses	$1.80 \times 10^{-5}$	$2.05 \times 10^{-5}$	12.2

$p_{d,t,\omega}$  is the load at bus  $d \in \mathcal{D}$ . Power flowing through the line  $(i, j) \in \mathcal{L}$  in scenario  $\omega$  is  $p_{ij,t,\omega}$  and the phase angle at bus  $i \in \mathcal{B}$  is denoted by  $\theta_{i,t,\omega}$ . Finally, the binary variables are denoted by  $z \in \{0, 1\}$  with an appropriate subscript to capture component shut-off decisions. We assume the objective function and subsequent constraints (except in Section III-B) are defined similarly to the author's prior work [10] in which a stochastic optimization is used.

Due to the uncertainty  $\omega$ , the objective function is stochastic, therefore, the SPSPS from [10] aims to minimize the expected economic costs,  $\Pi_\omega$ . However, we simplify the analysis using a scenario-based deterministic approach to solve the deterministic SPSPS described in Section III.F.

#### B. Constraint for Enacting No Less Than $k$ Damaged Lines with WLFP

Constraint (2) from the author's earlier work ([10]) represents a line shut-off strategy that constrains the total number of active lines so that the sum of each line risk's,  $R_{ij,t}$ , does not exceed  $R_{\text{tol}}$  which is an operator-driven parameter (measured in WFPI [16]).  $R_{\text{tol}}$  guarantees a certain level of security for the system while also penalizing the operation of transmission lines within regions of higher WFPI.

$$\sum_{(i,j) \in \mathcal{L}} z_{ij,t} R_{ij,t} \leq R_{\text{tol}}, \quad \forall t \in \mathcal{H} \quad (2)$$

In this work, we are measuring wildfire risk with the probability that a transmission line will experience damages from a nearby wildfire,  $\pi_{ij,t}$ . We use  $\pi_{ij,t}$  rather than  $R_{ij,t}$  to emphasize that our new transmission line wildfire risk is a probability rather than a unitless measure of vegetation flammability. As a result of changing the wildfire risk definition, the system wildfire risk budget constraint, previously

defined (2), must be redefined taking into account that wildfire ignitions are modeled as Bernoulli random events.

Overall, the degraded state of the system due to a specific combination of  $k$  line failures at time  $t$  is assumed to be the product of mutually independent events given by:

$$\mathbb{P}(\mathcal{L}) = \mathbb{P}(\mathcal{K} \cap \mathcal{K}^c) = \prod_{(i,j) \in \mathcal{K}} \pi_{ij,t} \prod_{(i,j) \in \mathcal{L} \setminus \mathcal{K}} 1 - \pi_{ij,t} \quad (3)$$

In Eq. 3,  $\mathcal{K}$  represents a set that contains which lines are damaged and  $\mathcal{K}^c$  (i.e. the complement of  $\mathcal{K}$ ) contains all lines that are undamaged. In this work, the constraint (2) is replaced with a non-linear constraint (4) to control  $z_{ij,t}^{\text{dn}}$  or  $k$  number of damaged lines:

$$\prod_{(i,j) \in \mathcal{K}} \pi_{ij,t}^{z_{ij,t}^{\text{dn}}} \prod_{(i,j) \in \mathcal{L} \setminus \mathcal{K}} (1 - \pi_{ij,t})^{z_{ij,t}} \leq \pi_{\text{tol}}, \quad (4)$$

$$z_{ij,t}^{\text{dn}} = z_{ij,t} - z_{ij,t-1} \quad \forall t \in \mathcal{H} \quad (5)$$

We reformulate this constraint as its linear counterpart by taking the log of both sides of the inequality as shown in (6),

$$\sum_{(i,j) \in \mathcal{K}} z_{ij,t}^{\text{dn}} \log(\pi_{ij,t}) + \sum_{(i,j) \in \mathcal{L} \setminus \mathcal{K}} z_{ij,t} \log(1 - \pi_{ij,t}) \leq \log(\pi_{\text{tol}}), \quad \forall t \in \mathcal{H} \quad (6)$$

### C. Day-ahead PSPS formulation

We use the deterministic PSPS formulation for the day-ahead stage of the PSPS optimization. The deterministic PSPS formulation is a special case of the stochastic PSPS problem from [10] in which it is assumed that the uncertainty is captured in a single scenario that represents the expected demand (i.e.  $\mathbb{E}[\mathbf{p}_{d,\omega}]$ ) and expected wildfire line risk (i.e.  $\mathbb{E}[\boldsymbol{\pi}_{ij,\omega}]$ ). The expected demand and wildfire risk are calculated  $\mathbb{E}[\mathbf{p}_{d,\omega}] = \sum_{\omega \in \Omega} \pi_{\omega} \mathbf{p}_{d,\omega}$  and  $\mathbb{E}[\boldsymbol{\pi}_{ij,\omega}] = \sum_{\omega \in \Omega} \pi_{\omega} \boldsymbol{\pi}_{ij,\omega}$  respectively.  $\pi_{\omega}$  is the probability of each scenario that contains both a daily demand curve and daily wildfire risk for every line. Since the deterministic DA optimization contains one scenario, we remove  $\omega$  subscripts from decisions variables. The resulting optimization problem with deterministic objective function ( $\Pi_{\text{DA}}$ ) for the day-ahead stage is given by,

$$\min_{z_{g,t}, z_{ij,t}, \mathbf{p}_g, \mathbf{x}_d} \Pi_{\text{DA}}, \quad (7)$$

s.t. Line Contingencies with  $\mathbb{E}[\boldsymbol{\pi}_{ij,\omega}]$ : (6),

$$z_{ij,t} \geq z_{ij,t+1} \quad \forall (i,j) \in \mathcal{L}, \quad (8)$$

$$z_{g,t} \geq \sum_{t' \geq t - t_g^{\text{MinUp}} \text{ to } t} z_{g,t'}^{\text{up}}, \quad (9)$$

$$1 - z_{g,t} \geq \sum_{t' \geq t - t_g^{\text{MinDn}}} z_{g,t'}^{\text{dn}}, \quad (10)$$

$$z_{g,t+1} - z_{g,t} = z_{g,t+1}^{\text{up}} - z_{g,t+1}^{\text{dn}}, \quad (11)$$

$$z_{g,t} \underline{p}_g \leq p_{g,t} \leq z_{g,t} \bar{p}_g, \quad (12)$$

$$p_{g,t}^{\text{aux}} = p_{g,t} - \bar{p}_g z_{g,t}, \quad (13)$$

$$\underline{U}_g \leq p_{g,t+1}^{\text{aux}} - p_{g,t}^{\text{aux}} \leq \bar{U}_g, \quad (14)$$

$$p_{ij,t} \leq -B_{ij} (\theta_{i,t} - \theta_{j,t} + \bar{\theta} (1 - z_{ij,t})), \quad (15)$$

$$p_{ij,t} \geq -B_{ij} (\theta_{i,t} - \theta_{j,t} + \underline{\theta} (1 - z_{ij,t})), \quad (16)$$

$$\underline{p}_{ij,t} z_{ij,t} \leq p_{ij,t} \leq \bar{p}_{ij,t} z_{ij,t}, \quad (17)$$

$$\sum_{g \in \mathcal{G}_i} p_{g,t} + \sum_{(i,j) \in \mathcal{L}} p_{ij,t} - \sum_{d \in \mathcal{D}_i} x_{d,t} \mathbb{E}[p_{d,t,\omega}] = 0, \quad (18)$$

$$\forall t \in \mathcal{H}, g \in \mathcal{G}, (i,j) \in \mathcal{L},$$

where the objective function consists of unit commitment costs ( $f^{\text{uc}}$ ), operational constraints ( $f^{\text{oc}}$ ), and value of lost load cost ( $f^{\text{VoLL}}$ ) as defined below,

$$\Pi_{\text{DA}} = f^{\text{uc}}(z_g^{\text{up}}, z_g^{\text{dn}}) + f^{\text{oc}}(\mathbf{p}_g) + f^{\text{VoLL}}(\mathbf{x}_d, \mathbb{E}[\mathbf{p}_{d,\omega}]), \quad (19)$$

$$f^{\text{uc}}(z_g^{\text{up}}, z_g^{\text{dn}}) = \sum_{t \in \mathcal{H}} \sum_{g \in \mathcal{G}} (C_g^{\text{up}} z_{g,t}^{\text{up}} + C_g^{\text{dn}} z_{g,t}^{\text{dn}}), \quad (20)$$

$$f^{\text{oc}}(\mathbf{p}_g) = \sum_{t \in \mathcal{H}} \sum_{g \in \mathcal{G}} C_g p_{g,t}, \quad (21)$$

$$f^{\text{VoLL}}(\mathbf{x}_d, \mathbb{E}[\mathbf{p}_{d,\omega}]) = \sum_{t \in \mathcal{H}} \sum_{d \in \mathcal{D}} C_d^{\text{VoLL}} (1 - x_{d,t}) \mathbb{E}[p_{d,t,\omega}]. \quad (22)$$

In (19)-(22),  $C_g^{\text{up}}$ ,  $C_g^{\text{dn}}$ , and  $C_g$  are the generator start up cost, shut down cost, and marginal cost respectively. The fraction of the load served is  $x_{d,t} \in [0, 1]$  and  $C_d^{\text{VoLL}}$  is the cost incurred as a result of shedding  $(1 - x_{d,t})$  proportion of the load,  $p_{d,t}$ . which together with the binary variables  $z_{g,t}^{\text{up}}$  and  $z_{g,t}^{\text{dn}}$  capture the one-time cost incurred when bringing a generator online or offline. Let  $p_g = (p_{g,1}, \dots, p_{g,H})^\top$  be the vector of  $p_{g,t}$  for generator  $g$ , then  $\mathbf{p}_g$  for all generators are denoted as  $\mathbf{p}_g = (p_1, \dots, p_G)^\top$ . The variables  $\mathbf{p}_d$ ,  $\mathbf{x}_d$ ,  $z_g^{\text{up}}$ ,  $z_g^{\text{dn}}$  are defined in a similar manner. In (8) it is assumed that when a line is switched off, it remains off for the remainder of the day. The unit commitment constraints (9)-(10) are used to enforce minimum up time ( $t_g^{\text{MinUp}}$ ) and down time ( $t_g^{\text{MinDn}}$ ) of generators. Similarly, the constraint (11) guarantees consistency between the binary variables  $z_{g,t}^{\text{up}}$  and  $z_{g,t}^{\text{dn}}$ . The power of generator  $g$  is limited between the minimum ( $\underline{p}_g$ ) and maximum ( $\bar{p}_g$ ) power generation limits of generator  $g$  in (12). Similarly, (13)-(14) implements the generator ramp rate limit between minimum ( $\underline{U}_g$ ) and maximum ( $\bar{U}_g$ ) limits. The auxiliary variable  $p_{g,t}^{\text{aux}}$  is introduced to prevent ramp violations during the startup process. To model power flow through the transmission lines, the DC-OPF approximation is used in (15)-(17) with minimum and ( $\underline{p}_{ij,t}$ ) maximum ( $\bar{p}_{ij,t}$ ) line thermal limits. Finally, the bus power balance at each  $t \in \mathcal{H}$  and every bus  $i \in \mathcal{B}$  is given by the equality constraint (18). The generation of the day-ahead scenarios  $\omega \in \Omega$  including a total demand and WIPs for every transmission line is further discussed in Section IV-A.

### D. Real-Time Outage Simulation

After the generator commitments and transmission line shut-off decisions are made, the system operator can test the performance of the commitment decisions against a realized demand at each node and the realized outage status of each transmission line.

Instead of optimizing costs over the expected demand and expected wildfire risk across scenarios  $\omega \in \Omega$ , realized

samples of demand and transmission line outages are used ( $p_{d,\omega'}$  and  $z_{ij,\omega'}$  respectively) where  $\omega' \in \Omega^{\text{RT}}$  are the realized scenarios. The real-time ignition probabilities,  $\pi_{ij,\omega'}$ , are used to generate 1,000 Monte Carlo samples of likely outage scenarios,  $z_{ij,\omega'}$ . In our analysis, we use one realization of demand (from the 1,000) and set each  $\pi_{\omega'} = \frac{1}{1,000}$ . In general, these realizations could also be drawn from a set of improved real-time forecast scenarios.

$$\min_{\mathbf{p}_{g,\omega'}, \mathbf{x}_{d,\omega'}} \sum_{\omega' \in \Omega^{\text{RT}}} \pi_{\omega'} \Pi_{\omega'} \quad (23)$$

s.t.

$$\Pi_{\omega'} = f^{\text{uc}}(\mathbf{z}_g^{\text{up}}, \mathbf{z}_g^{\text{dn}}) + f^{\text{oc}}(\mathbf{p}_{g,\omega'}) + f^{\text{VoLL}}(\mathbf{x}_{d,\omega'}, \mathbf{p}_{d,\omega'})$$

Generator Capacity Bounds with  $\mathbf{z}_g$ : (12)

Generator Ramping Constraints with  $\mathbf{z}_g$ : (13) – (14)

Optimal Power Flow Constraints with  $z_{ij,\omega'}$ : (15) – (17)

Real-time Demand Balance Constraints with  $\mathbf{p}_{d,\omega'}$ : (18)

$$i \in \mathcal{N}, \forall \omega' \in \Omega^{\text{RT}}, \forall t \in \mathcal{H}$$

#### IV. RESULTS

In this Section, we compare the cost performance of the deterministic PSPS framework based on whether the transmission line wildfire ignition probabilities (WIP) were predicted from WFPI or WLFP forecasts. Each day-ahead unit commitment is implemented on the IEEE RTS 24-bus system.

##### A. Data and Test Case Description

The grid model used for analysis is the modified IEEE RTS 24 bus system as shown in Fig. 1, consisting of 68 generating sources (3 wind generators, 20 roof-top PV (RTPV) clusters, 14 utility-scale PV units, 4 hydro, 1 synchronous condenser, 5 combined cycle (CC) generators, 15 combustion turbine (CT), 6 steam-powered generators), 17 loads, and 38 transmission lines. More information about the location, capacity, and costs of operation of each generator type can be obtained from [21]. The model is located within a region of Southern California near Los Angeles. The IEEE RTS 24 bus system is equivalent to the northwest region (i.e. Region 300) of the 73-bus RTS-GMLC [21]. The daily regional load profile given in Region 300 of the RTS GMLC system datasheet is projected onto a max-scaled version of the daily load experienced at each of the 24 bus locations [21].

Simulations on the IEEE RTS 24-bus system are performed over a full day and decisions are made hourly (i.e. 24 1-hour time steps). To determine representative scenarios for the PSPS optimization, total demand and bus level total wildfire risk (WFPI or WLFP) scenarios are generated via a tree reduction algorithm from [22]. The optimization horizon of interest is one day. The process of generating input data for the PSPS optimization in this paper is different than the process in the author's previous work [10] for two reasons. First, we now develop scenarios that contain information about total demand and cumulative wildfire risk rather than only total demand scenarios. In [10], the wildfire risk is deterministic and assumed to be the USGS day-ahead forecast for WFPI.

Next, WFPI values are now mapped to WIP due to replacing Constraint (2) with Constraint (6).

The tree scenario reduction method takes two inputs of the prior three months of demand forecasts for the total system load and of the cumulative WFPI/WLFP forecasts (averaged across all buses) for the region in which the 24 IEEE buses reside. We chose to create a joint distribution of total demand and cumulative bus WFPI/WLFP rather than total demand and cumulative line WFPI/WLFP. Line WFPI/WLFPs are an average risk over multiple climate zones while bus WFPI/WLFP represent more local wildfire risk measurements that can be related to the local demands at each bus. Each of the demand and WFPI/WLFP forecasts is sampled hourly. WFPI and WLFP are assumed constant throughout each day. The output of the scenario tree is the 5 most likely 24-hour total demand curves and their respective daily cumulative WFPI/WLFPs across all buses. The five total demand scenarios generated from the tree reduction algorithm are max-scaled and proportionally mapped to each of the static loads given in the IEEE RTS 24-bus system datasheet. A nearest neighbor (NN) search for each scenario is used to find which historical day's cumulative bus WFPI/WLFP is closest to each respective scenario's cumulative bus WFPI/WLFP.

The transmission line WFPI/WLFP values of those 5 historical days from the (NN) search are the transmission line WFPI/WLFP values for each respective scenario. The distribution of all WFPI/WLFP transmission line values for each scenario is shown in the box plot in Figures 6(c) and 6(d). Figures 6(a) and 6(b) provide the total demand timeseries for the 24 hour optimization horizon, and the probabilities of each respective scenario (top left of each total demand plot).

Using the projection method described above, we map the transmission line WFPI/WLFP values to WIP values based on the conditional mean OWIP provided in the USGS reliability diagrams. For our deterministic optimization problem, we take the expectation over the set of demand and WIP scenarios. The probability of each scenario can be seen in the bar charts

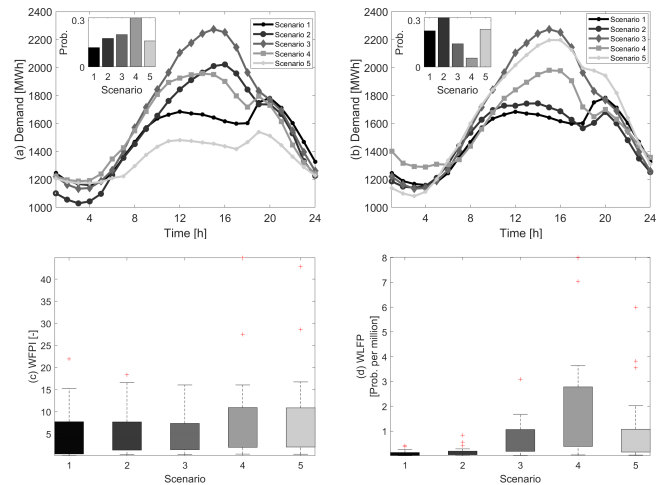


Fig. 6: Plot of the 5 scenarios for the IEEE 24-bus System derived from the tree reduction based on either WFPI (a) or WLFP (b) and load data from 2020. Box plots of the bus WFPI (c) and bus WLFP (d) for each scenario.

in Figures 6(a) and 6(b). Then, we optimize with the power balance constraint for the expected demand scenario (18) and one deterministic k-line damages constraint (6) for the expected WIP.

We test the robustness of each unit commitment strategy to real-time outages and demand uncertainties by defining the average available generation as a metric to compare the cost performance of each unit commitment strategy in real-time testing. The average available generation (AAG), defined in Eq. (24), is the total maximum capacity of all active generators averaged over the length of the optimization horizon,  $H$ .

$$\text{Ave. Avail. Gen.} = \frac{\Delta t}{H} \sum_{t \in \mathcal{H}} \sum_{g \in \mathcal{G}} \bar{p}_g z_{g,t}. \quad (24)$$

### B. Trends in Commitment and Day-ahead Operational Costs

In the simulations, the Value of Lost Load ( $C_d^{\text{VoLL}}$ ) is set to 1,000 \$/MWh for all demands [4], [23], [24]. Since the value of losing 1 MWh is at least one order magnitude higher than the cost to produce 1 MWh, the VoLL is typically the largest contributor to the total economic costs.

Simulation results for the day-ahead and real-time optimizations based on scenarios generated from WFPI and WLFPI forecasts are shown in Figure 7 and Figure 8 respectively. In the IEEE RTS 24 bus system, there are 38 lines, and 11 of those lines have zero risk. The  $\pi_{\text{tol}}$  is varied so that the average number of non-zero risk (NZR) line energizations optimized in the day-ahead optimization sweeps from 1 to 12 NZR active lines.

We reiterate that in the day-ahead optimization, the line de-energization decisions are chosen to not violate the tolerance,  $\pi_{\text{tol}}$ , in constraint (6). The NZR active line settings are the number of NZR active lines determined in the day-ahead optimization. However, in real-time the true line de-energization statuses are determined based on outage scenarios derived from the real-time WIP forecast. The real-time optimization model can experience an outage setting that is different than the day-ahead active line setting during the Monte Carlo simulation. From an operational perspective, only unit commitment decisions from the day-ahead optimization are carried over to the real-time optimization.

Table II shows the optimal value, WFPI/WLFP risk, and production cost per demand for different active line settings for both day-ahead (DA) optimization and real-time (RT) outage. The day-ahead optimization model with expected demand and transmission line wildfire risk based on WFPI forecasts experiences less expected demand (about 1.75% less) than the day-ahead model based on WLFPI; this leads to less total costs from commitment and production needed to serve that demand as well as less cost from possible load shed. As a result, lower day-ahead total economic costs (by 6.63% on average) are generated by the PSPS optimization when predicting WIP based on WFPI versus WLFPI as shown in Table II.

Due to the flexibility present in the IEEE RTS 24-bus system, only 12 (of the remaining 27) active lines with non-zero risk are needed for either strategy (using either WFPI or WLFPI forecasts to develop WIP) to satisfy their expected

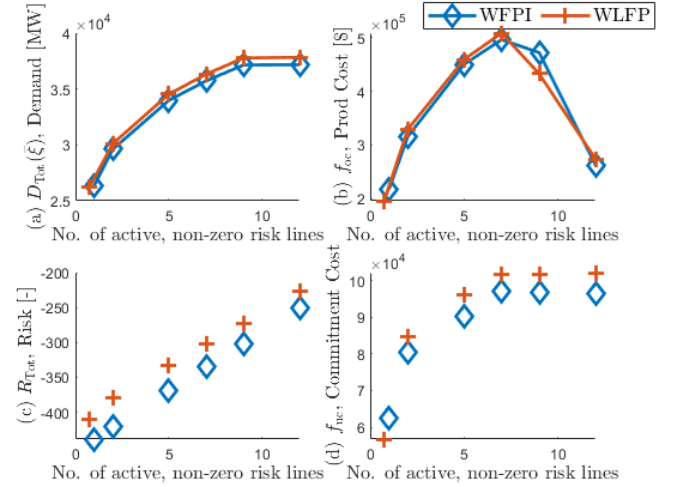


Fig. 7: Effect of the number of active lines on the a) day-ahead demand, b) day-ahead production costs, c) day-ahead wildfire risk, and d) commitment costs for the deterministic optimization approach. The wildfire risk scenarios were generated either from WFPI or WLFPI forecasts.

demand and achieve the minimum cost of serving the maximum amount of demand in the day-ahead model (Figure 7(a)). Both approaches achieve monotonic increases in demand with increases in active lines during the day-ahead optimization.

The day-ahead cumulative line wildfire risk depicted in Figure 7(c) and tabulated in Table II is computed by plugging the optimized line day-ahead de-energization decisions into the left-hand side of constraint (6) and summing log probabilities. The expected wildfire risk for the lines from WFPI forecasts is less in magnitude (Figure 7(c)) and is more uniformly distributed among scenarios (Figures 6(a) and 6(b)). The day-ahead optimized cumulative line wildfire risk is on average 10.14% less across the six different NZR active line settings based on WFPI forecasts (see middle part of Table II) than based on WLFPI forecasts. The underestimation of line wildfire risk by the WFPI forecasts allows for more lines to be activated under the same risk tolerance than allowed by the WLFPI forecasts. The greater uniformity in the wildfire forecasts among all transmission lines gives the operator greater flexibility in which lines to choose. An extreme example of uniformity in line risk would be the  $N-k$  approach (all lines are assigned the same amount of risk) which was shown in [10] to deliver the lowest costs among line contingency strategies. However, by underestimating the magnitude of each transmission line risk and variance in the distribution of transmission line risks across the network, the day-ahead unit commitment decisions made based on the WFPI forecasts tend to lead to higher total real-time costs than day-ahead unit commitment decisions based on WLFPI forecasts (as seen in Table II). The increase in real-time costs is due to the scenarios generated by WFPI forecasts not being an accurate representation of the true real-time demand and line outage probabilities as WLFPI forecasts.

The network structure greatly affects production and commitment costs. Both production and commitment costs increase from 1 to 7 NZR active lines, after which there is a decrease in both costs with 9 and 12 NZR active lines,



TABLE II: Difference in day-ahead and real-time total costs, cumulative wildfire risk, and production cost per demand between deterministic strategies that determine observed wildfire probability from WFPI and WLFPI forecasts

No. of NZR active lines	WFPI Value [\$1M]		WLFPI Value [\$1M]	
	DA	RT	DA	RT
12	0.35	2.12	0.38	0.6
9	0.56	0.48	0.83	0.46
7	7.51	0.48	8.29	0.48
5	16.11	1.01	17.21	0.52
2	37.67	4.14	39.17	1.82
1	53.46	17.61	58.46	18.63

No. of NZR active lines	WFPI Risk		WLFPI Risk	
	DA	RT	DA	RT
12	-250.62	-206.55	-225.99	-210.26
9	-301.39	-250.58	-273.34	-253.57
7	-335.46	-279.25	-301.55	-279.25
5	-368.83	-309.07	-333.07	-309.07
2	-419.94	-352.38	-378.76	-352.38
1	-438.49	-369.13	-409.61	-380.87

No. of NZR active lines	WFPI Prod per Dem. [\$/MWh]		WLFPI Prod per Dem. [\$/MWh]	
	DA	RT	DA	RT
12	7.06	6.99	7.24	7.16
9	12.71	9.26	11.49	8.74
7	13.90	9.26	14.00	9.11
5	13.26	9.00	13.31	8.99
2	10.66	8.23	10.93	8.29
1	8.24	5.87	7.47	5.90

as seen in the knee of the curve in Fig. 7(b) and (d). This trend is observed for the optimization based on WFPI and WLFPI forecasts. The decrease in production costs is due to the decrease in proportion of demand met by the more expensive CC and CT units and more of the production is being supplied by renewable sources. Whereas, the difference in commitment costs is due to the startup of the steam generator located at bus 16 which is explained in more depth in Section IV-D

### C. Trends in Commitment and Real-Time Operational Costs

Despite both Figure 7 and Table II (DA columns) showing that the model with WFPI forecasts resulted in less day-ahead cost in every active line setting, Figure 8 and Table II (RT columns) show that the commitment strategy from the model with WLFPI forecasts more often resulted in less real-time costs (5 out of the 6 active line settings). When the optimization based on WLFPI forecasts outperforms the optimization based on WFPI forecasts, the average real-time cost is 96.5% lower. When the optimization based on WFPI forecasts outperforms the optimization based on WLFPI forecasts, the average real-time cost is 5.47% lower. From Figure 8(a) we see that the WLFPI model served more demand in all cases except when there was only 1 non-zero active line. Because the expected demand differs and production cost scales with demand, Table II also shows the production costs per demand served. The production costs per MWh demand

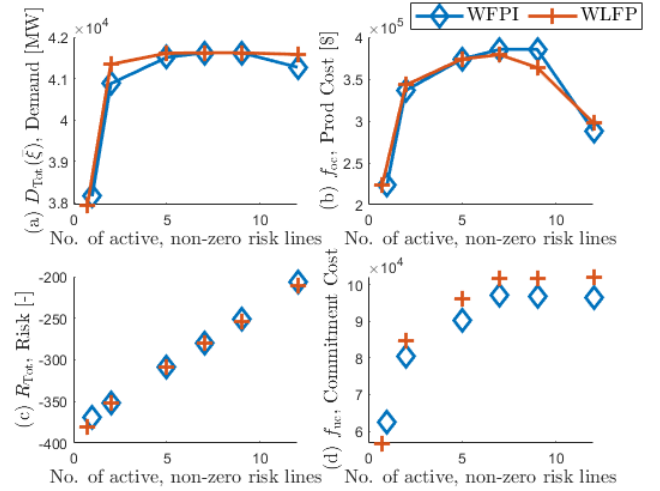


Fig. 8: Effect of the number of active lines on the a) expected real-time demand, b) expected real-time production costs, c) wildfire risk, and d) commitment costs for the deterministic optimization approach. The wildfire risk scenarios were generated either from WFPI or WLFPI forecasts. The testing day was with July 31st, 2020.

for WLFPI model is on average 2.62% less for NZR active line settings of 5, 7, and 9 and 1.22% more for the NZR active line settings of 1, 2, and 12 than the WFPI model. The wildfire risk in Figure 8 and RT columns in Table II is computed via the left-hand side of Eq. (6) with the real-time observed probability forecast on July 31st and the de-energization decisions made in the day-ahead optimization.

### D. Difference in Average Available Generation based on the optimization with WFPI and WLFPI forecasts

In Figure 9, we use the trend in average available generator capacity (defined in Eq. (24)) versus the number of day-ahead NZR active lines to explain how day-ahead unit commitments impact the PSPS optimization model's robustness to the real-time line outages.

As the number of day-ahead NZR active lines increases from 1 to 7, there is a decrease in overall costs and an increase in average available generation. This is because as more active lines are added to the network there is more opportunity for generation to occur without saturating the power flow on the lines. However, the least costly real-time solution does not occur at the greatest number of active lines or the maximum amount of generation capacity; the least costly solution occurs at the 9 NZR active line setting. The 7 NZR active line setting commits more generators than necessary during 1700 h to 2400 h to serve the full real-time area demand. Whereas, there is a slight increase in costs when 12 non-zero risk lines are active due to a more risk-seeking commitment strategy. Since at least 12 non-zero active lines are needed to fully serve the day-ahead demand, the active line setting of 12 or more lines aggressively reduces the generation capacity of units committed throughout the day. During 1000 h to 1500 h, the AAG can be decreased by nearly 400 MW or 8.3%. This reduction of generation capacity in the day-

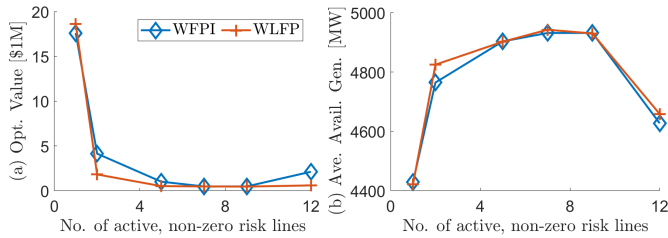


Fig. 9: Optimal expected total real-time costs versus the number of active lines with non-zero line risk (a) and the average maximum available generation versus the number of active lines with non-zero line risk (b) when scenarios were reduced using WFPI (diamond) and WLPF (plus) data

ahead 12 non-zero active line setting leads to a shortage of necessary generation capacity to serve all the real-time demand regardless of the wildfire risk metric used. However, the day-ahead optimization model with scenarios based on WFPI forecasts is most affected.

## V. CONCLUSION

This paper shows how an operator's choice of wildfire risk metric influences the optimal unit commitment decisions during PSPS. A deterministic version of the SPSPS framework (from the author's previous work [10]) is used to minimize total economic costs and is implemented on the IEEE RTS 24-bus system in two stages. We select two WIP forecasting models: one uses transmission line WFPI to predict transmission line WIP and the other uses transmission line WLPF to predict transmission line WIP.

Expected total grid demand and expected WIP at each transmission line across the 5 representative days is used as an input in a day-ahead unit commitment optimization. In the first stage of the optimization (i.e. in the day ahead), we select the unit commitment decisions. Then in the second stage (i.e. real-time) we test the unit commitment decisions via a Monte Carlo simulation across the real-time demand and a collection of possible real-time transmission line outage scenarios. The expected transmission line WIP and demand scenarios generated with WFPI forecasts and total demand underestimate the expected real-time transmission line WIP and expected total demand. This underestimation of demand and WIP leads to day-ahead unit commitments whose generator fleet has less real-time output and is less robust to real-time outage scenarios. This lack of robustness in the unit commitment decisions optimized over WIP values from the WFPI forecasts often lead to higher average real-time costs.

This study is limited to showing the impact of the two main wildfire risk metrics (released by the USGS) on PSPS optimization. Additional studies may be needed to show how the PSPS optimization's total economic cost would be affected by wildfire forecasts developed by utilities or by other proposed methods in the literature (e.g. the wildfire forecasting methods developed in [11]–[13]).

## REFERENCES

[1] B. Isaacs-Thomas, "California's catastrophic wildfires in 3 charts," PBS News, Sep. 14, 2020. <https://www.pbs.org/newshour/science/california-catastrophic-wildfires-in-3-charts> (accessed Jul. 10, 2024).

[2] California Public Utilities Commission. Public Safety Power Shut-off (PSPS)/De-Energization. Accessed: Oct. 2020. [Online]. Available: <https://www.cpuc.ca.gov/deenergization>

[3] A. Arab, A. Khodaei, R. Eskandarpour, M. P. Thompson and Y. Wei, "Three Lines of Defense for Wildfire Risk Management in Electric Power Grids: A Review," in *IEEE Access*, vol. 9, pp. 61577-61593, 2021, doi: 10.1109/ACCESS.2021.3074477.

[4] D. N. Trakas and N. D. Hatzigiorgiou, "Optimal Distribution System Operation for Enhancing Resilience Against Wildfires," in *IEEE Transactions on Power Systems*, vol. 33, no. 2, pp. 2260-2271, March 2018, doi: 10.1109/TPWRS.2017.2733224.

[5] N. Rhodes, L. Ntaimo and L. Roald, "Balancing Wildfire Risk and Power Outages Through Optimized Power Shut-Offs," in *IEEE Transactions on Power Systems*, vol. 36, no. 4, pp. 3118-3128, July 2021, doi: 10.1109/TPWRS.2020.3046796.

[6] A. Kody, R. Piansky, and D. Molzahn, "Optimizing Transmission Infrastructure Investments to Support Line De-energization for Mitigating Wildfire Ignition Risk," in *11th Bulk Power Systems Dynamics and Control Symposium (IREP XI)*, Banff, Canada, July 2022.

[7] N. Rhodes, C. Coffrin, and L. Roald, "Security constrained optimal power shutoff for wildfire risk mitigation," *IET Generation, Transmission, & Distribution*, 2024

[8] A. Kody, A. West, and D. Molzahn, "Sharing the Load: Considering Fairness in De-energization Scheduling to Mitigate Wildfire Ignition Risk using Rolling Optimization." Accessed: Oct. 24, 2022. [Online]. Available: <https://arxiv.org/pdf/2204.06543.pdf>

[9] Han. Yang, N. Rhodes, Hao. Yang, L. Roald, and L. Ntaimo, "Multi-period Power System Risk Minimization under Wildfire Disruptions", in *IEEE Transactions on Power Systems*, doi: 10.1109/TPWRS.2023.3339147.

[10] R. Greenough, K. Murakami, M. R. Davidson, J. Kleissl, A. Khurram, "Wildfire Resilient Unit Commitment under Uncertain Demand," arXiv preprint, 2403.09903, 2024.

[11] A. Umunnakwe, M. Parvania, H. Nguyen, and J. D. Horel, and K. R. Davis, "Data-driven spatio-temporal analysis of wildfire risk to power systems operation," 2021.

[12] R. Bayani, M. Waseem, S. D. Manshadi and H. Davani, "Quantifying the Risk of Wildfire Ignition by Power Lines Under Extreme Weather Conditions," in *IEEE Systems Journal*, vol. 17, no. 1, pp. 1024-1034, March 2023, doi: 10.1109/JSYST.2022.3188300.

[13] R. Bayani and S. D. Manshadi, "Resilient Expansion Planning of Electricity Grid Under Prolonged Wildfire Risk," in *IEEE Transactions on Smart Grid*, vol. 14, no. 5, pp. 3719-3731, Sept. 2023, doi: 10.1109/TSG.2023.3241103.

[14] "Fire Hazard Severity Zones — OSFM," Ca.gov, 2024. <https://osfm.fire.ca.gov/what-we-do/community-wildfire-preparedness-and-mitigation/fire-hazard-severity-zones> (accessed Aug. 20, 2024).

[15] "Reliability diagrams of the WFPI model — U.S. Geological Survey," Usgs.gov, 2017. <https://www.usgs.gov/media/images/reliability-diagrams-wfpi-model> (accessed Jul. 12, 2024).

[16] Wildland Fire Potential Index, U.S. Geological Survey. <https://www.usgs.gov/fire-danger-forecast/wildland-fire-potential-index-wfpi>

[17] WFPI-based Large Fire Probability, U.S. Geological Survey. <https://www.usgs.gov/fire-danger-forecast/wfpi-based-large-fire-probability-wlfp>

[18] K. C. Short, "Spatial wildfire occurrence data for the United States," 1992-2020 [FPA\_FOD\_20221014]. 6th Edition. Fort Collins, CO, 2022: Forest Service Research Data Archive. <https://doi.org/10.2737/RDS-2013-0009.6>.

[19] Wikipedia Contributors, "2015 California wildfires," Wikipedia, Jun. 28, 2024. (accessed Jul. 25, 2024).

[20] "ICS183: Bresenham's algorithm," CS 112: Computer Graphics, University California Irvine Information and Computer Science Department, <https://ics.uci.edu/~gopi/CS112/web/handouts/OldFiles/Bresenham.pdf>

[21] "Reliability Test System Grid Modernization Lab Consortium (RTS-GMLC) Transmission System Database," Grid Modernization Lab, (2022). <https://github.com/GridMod/RTS-GMLC>

[22] N. Gröwe-Kuska, H. Heitsch, and W. Römisch, "Scenario reduction and scenario tree construction for power management problems," in *2003 IEEE Bologna PowerTech*, 2003, vol. 3, pp. 152-158.

[23] S. Mohagheghi and S. Rebennack, "Optimal resilient power grid operation during the course of a progressing wildfire," *Int. J. Elect. Power Energy Syst.*, vol. 73, pp. 843-852, 2015.

[24] H. Farzin, M. Fotuhi-Firuzabad, and M. Moeini-Aghtaie, "Stochastic energy management of microgrids during unscheduled islanding period," *IEEE Trans. Ind. Informat.*, vol. 13, no. 3, pp. 1079-1087, Jun. 2017.